Journal of Advanced Ceramics
2015, **4**(2): 94–102
DOI: 10.1007/s40145-015-0141-5

ISSN 2226-4108
CN 10-1154/TQ

Research Article

Preparation, mechanical, and thermal properties of a promising thermal barrier material: $Y_4Al_2O_9$

Yanchun ZHOU*, Xinpo LU, Huimin XIANG, Zhihai FENG

Science and Technology of Advanced Functional Composite Laboratory, *Aerospace Research Institute of Materials and Processing Technology*, *No. 1 South Dahongmen Road*, *Beijing 100076*, *China*

Received: January 26, 2015; Accepted: February 02, 2015

Abstract: In our previous work, anisotropic chemical bonding, low shear deformation resistance, damage tolerance ability, low thermal conductivity, and moderate thermal expansion coefficient of $Y_4Al_2O_9$ (YAM) were predicted. In this work, phase-pure YAM powders were synthesized by solid-state reaction between Y_2O_3 and Al_2O_3 and bulk YAM ceramics were prepared by hot-pressing method. Lattice parameters and a new set of X-ray powder diffraction data were obtained by Rietveld refinement. The mechanical and thermal properties of dense YAM ceramics were investigated. The measured elastic moduli are close to the theoretical predicted values and the stiffness can be maintained up to 1400 ℃. The flexural strength and fracture toughness are 252.1±7.3 MPa and 3.36±0.20 MPa·m$^{1/2}$, respectively. Damage tolerance of YAM was also experimentally proved. The measured average linear thermal expansion coefficient (TEC) of YAM is 7.37×10^{-6} K^{-1}, which is very close to the theoretical predicted value. Using high-temperature X-ray diffraction (XRD) analysis, volumetric TEC is determined $(23.37\pm1.61)\times10^{-6}$ K^{-1} and the anisotropic TEC are $\alpha_a = 7.34\times10^{-6}$ K^{-1}, $\alpha_b = 7.54\times10^{-6}$ K^{-1}, and $\alpha_c = 7.61\times10^{-6}$ K^{-1}.

Keywords: $Y_4Al_2O_9$; X-ray diffraction (XRD) pattern; mechanical properties; thermal expansion; damage tolerance

1 Introduction

Previous theoretical [1–3] and experimental [4,5] investigations have demonstrated that $Y_4Al_2O_9$ (YAM) has a unique combination of high melting point (2020 ℃), low density (4.44 g/cm^3), low high-temperature thermal conductivity (the minimum thermal conductivity is 1.13 W·m^{-1}·K^{-1}), relative low Young's modulus (191 GPa), and moderate thermal expansion coefficient (7.51×10^{-6} K^{-1}) and damage tolerant ability, which endure it as a prospective material for thermal and/or environmental barrier coating applications. However, besides Young's modulus and thermal conductivity, other mechanical and thermal properties have not been experimentally explored. In addition, the experimental lattice parameters are from high-temperature neutron diffraction study at 1791 K, which are obviously larger than the room temperature data. Since these properties are indispensable for the selection and application of YAM as a candidate material for thermal barrier coating (TBC) applications, it is necessary to systematically investigate the structural, thermal, and mechanical properties of YAM.

The purpose of this work is to provide the

* Corresponding author.
E-mail: yczhou@imr.ac.cn

experimental determined lattice parameters and mechanical and thermal properties of dense phase-pure YAM. To achieve such a goal, single-phase YAM powders were prepared by solid-state reaction between Y_2O_3 and Al_2O_3 first. Then near fully dense YAM sample was prepared by hot-pressing the YAM powders at 1800 ℃. The lattice constants, atomic positions, and a new set of X-ray powder diffraction patterns were obtained by Rietveld refinement. The average linear thermal expansion coefficient (TEC) was measured by using an optical dilatometer, and the anisotropic thermal expansion coefficients at different directions were determined by high-temperature X-ray diffraction. The Vickers hardness, flexural strength, fracture toughness, and dynamic Young's modulus were also measured. These fundamental data are helpful for promoting the applications of YAM as a TBC material or high-temperature structural component.

2 Experimental procedure

To investigate the thermal and mechanical properties of YAM, near fully dense and phase-pure samples are needed. These samples were prepared by the following steps. First, phase-pure YAM powders were synthesized by a solid-state reaction method using yttria powders (Y_2O_3, 99.9% purity; Yuelong Reagent Co., Shanghai, China) and alumina powders (Al_2O_3, 99.9% purity; Yuelong Reagent Co., Shanghai, China) as starting materials. To synthesize single-phase YAM, powders with the mole ratio of Y_2O_3: Al_2O_3 = 2:1 were mixed and then calcined at 1500 ℃ for 2 h in air. Bulk YAM samples with 50 mm in diameter were prepared by hot-pressing the as-synthesized YAM powders at 1800 ℃ under a pressure of 30 MPa for 60 min in a flowing Ar atmosphere.

Phase compositions of the as-synthesized YAM powders and bulk YAM samples were identified by a step-scanning X-ray diffractometer (Brook D8; Germany) with Cu Kα radiation (λ = 1.54178 Å). The lattice parameters, atomic positions, 2θ, *hkl*, and peak intensities of YAM were refined by the Rietveld method [6,7] (Topas software, Bruker, Germany). The reliability factors R_p and R_{wp} were calculated by

$$R_p = \frac{\sum_i |cY_{sim}(2\theta_i) - I_{exp}(2\theta_i) + Y_{back}(2\theta_i)|}{\sum_i |I_{exp}(2\theta_i)|} \quad (1)$$

$$R_{wp} = \left\{ \frac{\sum_i w_i [cY_{sim}(2\theta_i) - I_{exp}(2\theta_i) + Y_{back}(2\theta_i)]^2}{\sum_i w_i [I_{exp}(2\theta_i)]^2} \right\}^{1/2} \quad (2)$$

where $w_i = 1/I_{exp}(2\theta_i)$ is a weighting function; c the constant scaling factor optimized to obtain the lowest value of R_{wp}; $I_{exp}(2\theta_i)$ the measured experimental spectrum; $Y_{back}(2\theta_i)$ the background intensity of the measured spectrum; and $Y_{sim}(2\theta_i)$ the simulated diffraction intensity without the background contribution. The intensity was calculated by

$$I_{Rietveld}(2\theta) = b(2\theta) + S\sum_k L_k |F_k|^2 \phi(2\theta_i - 2\theta_k) P_k A_k \quad (3)$$

where $b(2\theta)$ is the background intensity; S the scaling factor; L_k contains the Lorentz polarization and multiplicity factors; ϕ the profile function; P_k the preferred orientation function; A_k absorption factor; and F_k the structure factor. The index k presents Miller indices for the Bragg reflections.

Microstructure observations were conducted in an Apollo 300 scanning electron microscope (SEM; CamScan Co., England). Before microstructure investigation, the samples were polished and thermally etched at 1100 ℃ for 1 h in air.

The density of the bulk YAM ceramics was measured by the Archimedes method. The Vickers hardness was measured at a load of 10 N with a dwell time of 15 s. The flexural strength was determined via an three-point bending test method using samples with the dimension of 3 mm × 4 mm × 36 mm. The fracture toughness K_{IC} was measured using single-edge notch beam (SENB) specimens with the dimension of 4 mm × 8 mm × 36 mm. The notch with the size of 4 mm in length and 0.10 mm in width was made by a diamond coated wheel slotting. The crosshead speed was 0.5 mm/min and 0.05 mm/min for flexural strength and fracture toughness measurement, respectively. The elastic modulus was evaluated by the impulse excitation technique using a rectangular sample with the dimension of 3 mm × 15 mm × 40 mm. The sample was given a mechanical impulse, and the vibration was detected by a microphone and then analyzed with the resonance frequency and damping analyzer (Resonance Frequency and Damping Analyzer, IMCE, Diepenbeek, Belgium), which is a standard testing method for dynamic Young's modulus, shear modulus, and Poisson's ratio by sonic resonance. The Young's modulus was calculated from the flexural

resonate frequency, f_F, according to ASTM E 1876-97 [8]:

$$E = 0.9465\left(\frac{mf_F^2}{w}\right)\left(\frac{L^3}{t^3}\right)T_1 \quad (4)$$

with E the dynamic elastic modulus; f_F the fundamental flexural resonant frequency; m, w, L, and t the mass, width, length, and thickness of the specimen. T_1 is a correction factor, depending on the Poisson's ratio υ and the thickness/length ratio t/L.

Temperature dependence of Young's modulus and internal friction of YAM ceramics was measured in a graphite furnace at a heating rate of 4 ℃/min in flowing argon atmosphere. The sample was suspended in the nodes of their first bending vibration mode (0.024L apart from both ends of rectangular beam, where L is the sample length). The vibration signal captured by a laser vibrometer was analyzed with the frequency and damping analyzer [9]. The internal friction corresponding to the flexural vibration mode was calculated as $Q^{-1}=k/(\pi f_F)$, where k is the exponential decay parameter of the amplitude of the flexural vibration component. Detailed testing process can be found in our previous work [10].

The average linear thermal expansion coefficient (TEC) of YAM was obtained from the temperature dependent changes of the length of the specimen from room temperature to 1600 K in air by using a vertical high-temperature optical dilatometer (ODHT-1600-50, Expert System Solutions, Modena, Italy). The specimen used was a rectangular bar with the dimension of 3 mm in width, 4 mm in length, and 15 mm in height. The height direction is perpendicular to the hot-pressing direction. A sharp edge was made on top end of the height of the test specimen. During testing, the sample was put in a furnace using Pt as heating element and the top sharp end of the specimen was aligned by one optical path, and the sample holder was focused by another optical path, which was taken as a reference beam to correct the mechanical drift of the instrument. The data were continuously collected by a personal computer during heating at a rate of 5 K/min.

To investigate the anisotropic thermal expansion behavior of YAM, high-temperature X-ray diffraction (XRD) was performed on YAM powder samples utilizing Cu Kα radiation with a step size of 0.02° at scanning rate of 1 (°)/min. The data were collected from a high-temperature diffractometer (X' Pert-ProMPD; PANalytical, Almelo, the Netherland) in 2θ range between 15° and 45° during a stepwise heating to 1273 K with a step width of 100 K. The heating rate was 10 K/min and the dwell time was 15 min before each test. The XRD patterns for each 100 K interval in temperature were refined using the Rietveld method (TOPAS software; Bruker, Germany) and the lattice parameters were obtained. The anisotropic TECs of YAM were determined by fitting the lattice constants versus temperature curves.

3 Results and discussion

3.1 Phase composition and microstructure

The XRD pattern of $Y_4Al_2O_9$ (YAM) powders prepared by solid-state reaction method at 1500 ℃ for 2 h is shown in Fig. 1(a). One can see from the figure that the as-prepared YAM is phase-pure without any impurities detectable by XRD. Since the previous determined lattice parameters and atomic positions are from high-temperature neutron diffraction at 1791 K [11], which are different from the room temperature data due to thermal expansion, Rietveld refinement was performed to obtain the lattice constants, atomic positions, and intensities of YAM. The lattice constants are $a=7.3865$ Å, $b=10.4750$ Å, $c=11.1251$ Å, and $\beta=108.6264°$. The final reliability factors for Rietveld refinement are $R_p=5.89\%$ and $R_{wp}=8.39\%$. The lattice constants are slightly smaller than the previously neutron diffraction determined values, which is due to the temperature caused expansion in previous work [11]. The atomic positions are given in Table 1. Since these data are obtained at room temperature, it is more reliable and useful in further phase identification and structure analysis. The reflections and intensities for the experimental and calculated XRD patterns are listed in Table 2. It is seen from Table 2 that the calculated peak positions are agreed well with the observed ones. The intensities are also agreed with the experimental observed ones. Thus this new set of XRD data is reliable and useful for further phase identifications.

Figure 1(b) shows the XRD pattern of the bulk YAM hot-pressed at 1800 ℃. It is obvious that the bulk YAM sample is also phase-pure, which indicates that YAM is stable without decomposition at high temperatures even up to 1800 ℃. The relative intensities of the reflections in Fig. 1(a) and Fig. 1(b)

are almost identical, except that the (220) and (040) peaks become slightly stronger, demonstrating that there is no strong preferred orientation of the hot-pressed YAM sample. Figure 2 shows the microstructure of the polished and thermally etched surface of the hot-pressed YAM sample. No residual pores can be seen in the observed region, indicating that the bulk YAM sample is near fully dense. The density determined by Archimedes method is about 99% of the theoretical. The grains are equiaxial in morphology with an average grain size of about 4 μm. Carefully checking the microstructure, one can find that there is a small quantity of nanometer-sized Y_2O_3 at the grain boundary of YAM (white nanometer-sized particles in the figure, confirmed by energy-dispersive X-ray spectroscopy), which cannot be detected by XRD. The influence of these nanometer-sized Y_2O_3 particles on the mechanical properties of YAM is not clear and we will discuss it in the later sections.

Table 1 Lattice constants and atomic positions of YAM

	Lattice constant
a (Å)	7.3865
b (Å)	10.4750
c (Å)	11.1251
β (°)	108.6264
	Atomic position
Al(1)	(0.9402, 0.1780, 0.1276)
Al(2)	(0.3970, 0.1860, 0.1060)
Y(1)	(0.2663, 0.0852, 0.8018)
Y(2)	(0.7988, 0.0967, 0.8064)
Y(3)	(0.0606, 0.1388, 0.4274)
Y(4)	(0.5914, 0.1229, 0.4307)
O(1)	(0.5240, 0.2210, 0.7467)
O(2)	(0.9860, 0.2110, 0.7794)
O(3)	(0.9400, 0.0039, 0.1396)
O(4)	(0.8343, 0.2499, 0.9824)
O(5)	(0.1780, 0.2145, 0.1180)
O(6)	(0.3870, 0.2470, 0.9758)
O(7)	(0.4779, 0.0368, 0.1847)
O(8)	(0.8374, –0.0086, 0.3811)
O(9)	(0.3402, –0.0165, 0.3883)

Table 2 Reflections, 2*θ*, and intensities data of YAM from experiment (Obs.) and Rietveld refinement (Cal.)

Reflection *hkl*	$2\theta_{\text{Obs.}}$ (°)	$2\theta_{\text{Cal.}}$ (°)	$I/I_{0\,\text{Obs.}}$ (%)	$I/I_{0\,\text{Cal.}}$ (%)
(011)	11.92	11.90	15.4	15.1
(002)	16.86	16.86	3.4	1.5
(020)	16.94	16.94	3.0	1.3
(012)	18.84	18.86	25.1	27.6
(111)	19.20	19.24	2.1	2.4
(022)	24.02	24.00	10.2	10.8
(102)	24.16	24.14	4.6	5.0
$(20\bar{2})$	25.66	25.66	2.4	2.4
(103)	26.80	26.78	31.4	32.6
$(2\,\bar{1}\,2)$	27.10	27.08	2.7	2.4
$(2\bar{2}\,\bar{1})$	29.60	29.64	100.0	100.0
(023)	30.70	30.68	92.5	98.7
(040)	34.28	34.28	29.8	29.8
(202)	35.02	35.06	12.6	12.1
(041)	35.32	35.32	7.8	7.8
$(20\bar{4})$	35.52	35.52	13.5	14.4
(033)	36.30	36.32	8.5	7.8
$(2\,\bar{1}\,4)$	36.52	36.50	9.1	9.1

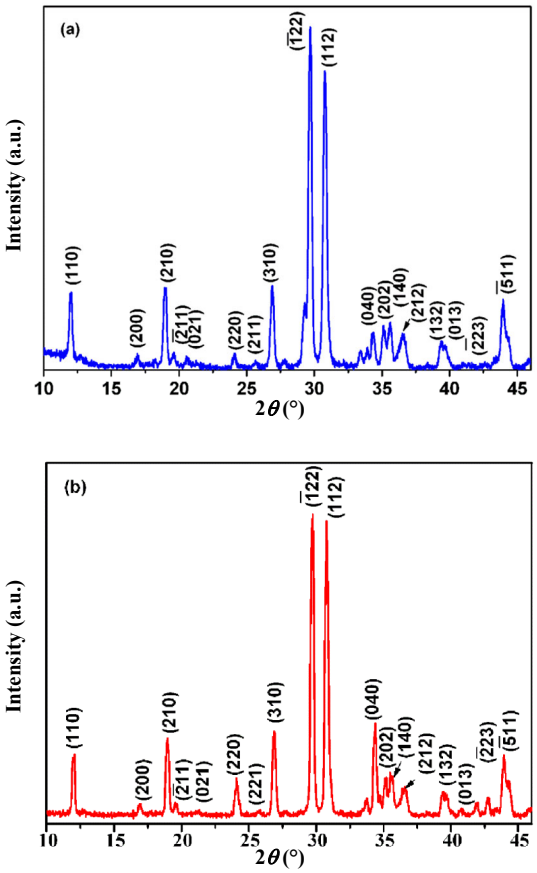

Fig. 1 XRD patterns of (a) as-synthesized YAM powders and (b) hot-pressed YAM at 1800 ℃.

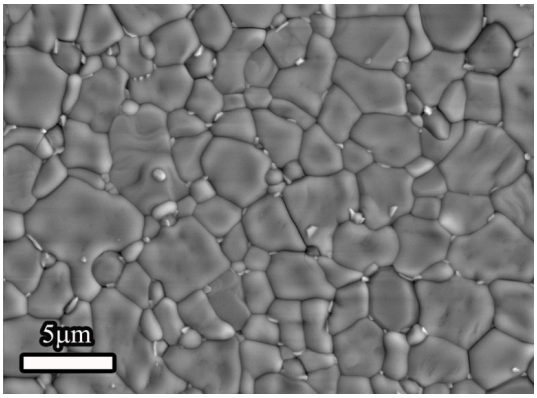

Fig. 2 SEM micrograph of etched surface of hot-pressed YAM.

3. 2 Room temperature mechanical properties

The measured mechanical and thermal properties of $Y_4Al_2O_9$ are summarized in Table 3. The measured room temperature Young's modulus E and shear modulus G are 204 GPa and 80 GPa, respectively, which are slightly higher than but still close to the theoretical predicted values of 191 GPa and 76 GPa, respectively. The higher Young's modulus can be attributed to the presence of a small amount of Y_2O_3 at the grain boundary, because Y_2O_3 has higher Young's modulus. The measured Poisson's ratio υ is 0.27, which is also close to the theoretical predicted value of 0.26. The consistency between the theoretical calculated and the experimental measured elastic properties demonstrates the high reliability of our density functional theory (DFT) calculations [2]. In our previous work [2], YAM was predicted to be a damage tolerant ceramic based on the low Pugh's ratio G/B = 0.576. Using the experimentally measured shear modulus and bulk modulus, the Pugh's ratio is calculated to be G/B = 0.530, which is also close to the theoretical value, confirming the damage tolerance of YAM.

The measured Vickers hardness of YAM is 11.02±0.33 GPa, which almost equals to the average of the hardness of Y_2O_3 (6.8 GPa) and Al_2O_3 (21 GPa) and is close to the theoretical value of 10.2 GPa predicted using the empirical model of Chen *et al.* [12]. The flexural strength and fracture toughness were also measured. The flexural strength is 252.1±7.3 MPa and the fracture toughness is 3.36±0.20 MPa·m$^{1/2}$. Relatively high fracture toughness to strength ratio indicates the damage tolerance ability of YAM. Bao *et al.* [13] proposed an equation as a quantitative measure of damage tolerance:

$$D_t = \frac{K_{IC} \cdot E}{\sigma_b \cdot H} \quad (5)$$

High D_t indicates good damage tolerance. Putting the measured hardness, Young's modulus, strength, and fracture toughness data into Eq. (5), the damage tolerance of YAM is determined 0.25. This value is slightly lower than those of β-$Yb_2Si_2O_7$ (0.39) [14] and γ-$Y_2Si_2O_7$ (0.37) [15], but still warants the damage tolerance of YAM.

To understand the mechanism of damge tolerance, the fracture surfaces were examined by SEM. Figure 3 shows the fracture surfaces of YAM; wherein layered characteristics are obvious, which are similar to those observed on the fracture surfaces of Ti_3SiC_2 [16] and other layered ternary carbides and nitrides [17–20]. The delamination of YAM grains results in the formation of nanolaminated layers on the fracture surfaces, such as the area labeled A, B, and C in Fig. 3(a) and D, E, and F in Fig. 3(b). The formation of nanolayered layers on the fracture surfaces is mainly due to anisotropic bonding and the presence of weakly bonded atomic planes [2]. We have shown through DFT calculations that the anisotropic elastic moduli are E_x = 208 GPa, E_y = 179 GPa, and E_z = 176 GPa. The maximum and minimum Young's modulus are 210 GPa and 170 GPa, respectively. The high- and low-directions correspond to the high- and low-fracture-energy directions. Thus, shear-induced sliding along the low Young's modulus directions like $(0\bar{1}1)/[0\bar{1}1]$ or (011)/[011] forms nanolayered cleavage steps on the fracture surfaces [2]. From the crystal structure shown in our previous work [2] and the crystallite shape of YAM simulated based on the Donnay–Haker theory [21–23], $\{0\bar{1}1\}$, {011}, and {100} planes are of morphological importance in crystal morphology of YAM. The crystallite shapes observed by SEM in Fig. 2, Fig. 3(a), and Fig. 3(b) are identical to those viewed in different directions as shown in Fig. 3(c) and Fig. 3(d). The angle between the weakly bonded $(0\bar{1}1)$ and (011) planes is 86.7°. In grains labeled A and B in Fig. 3(a) and D and E in Fig. 3(b), delamination occurs on the two weakly bonded $(0\bar{1}1)$ and (011) planes simultaneously. Also the nanolaminated layers formed by shear-induced sliding along the first weakly bonded planes ($(0\bar{1}1)/[0\bar{1}1]$ or (011)/[011]) are "cut" by the second weakly bonded planes ((011)/[011] or $(0\bar{1}1)/[0\bar{1}1]$). The formation of nanolaminated grains and sliding of the nanometer-thick thin slabs along the weakly bonded planes consumes energy and contributes to the damage tolerance of YAM [2].

Table 3 Summary of mechanical and thermal properties of YAM

σ_b (MPa)		H_V (GPa)	K_{IC} (MPa·m$^{1/2}$)	E (GPa)	G (GPa)	υ	TEC (10^{-6}K^{-1})
R.T.	1200 ℃	R.T.	R.T.	R.T.	R.T.	R.T.	300–1500 K
252.1±7.3	104.2±8.6	11.02±0.33	3.36±0.20	204	80	0.27	7.37

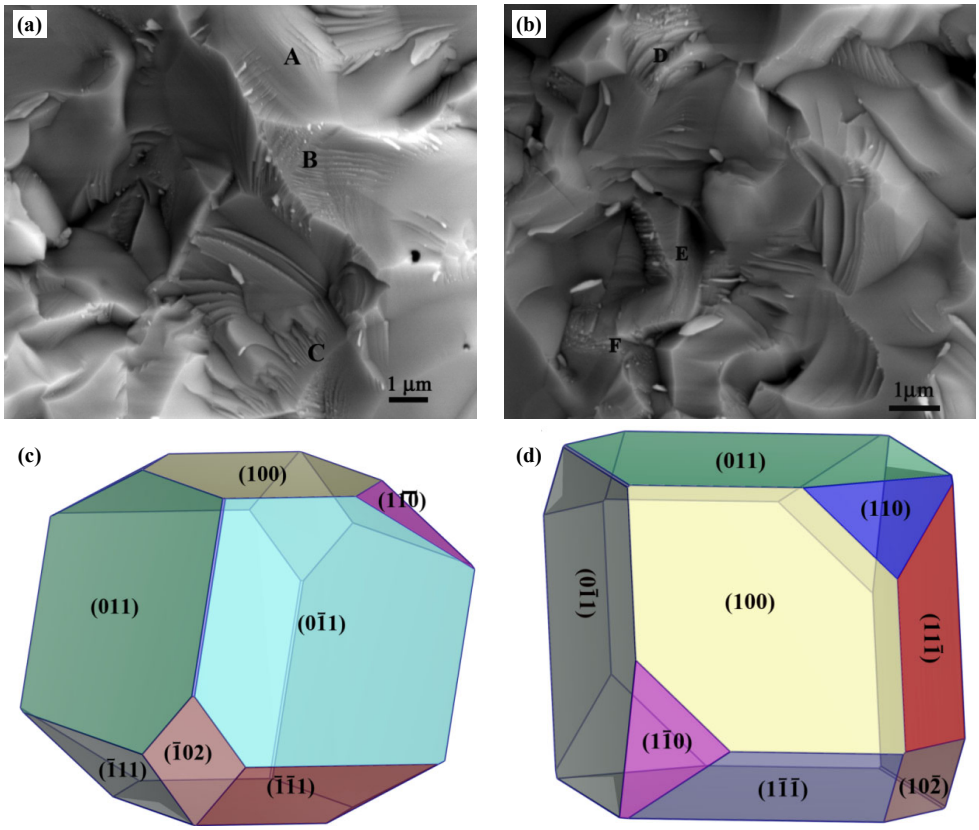

Fig. 3 (a) and (b) Fracture surfaces of YAM. Nanolaminated layers are formed are due to the presence of weakly bonded planes. Delaminating occurs on two weakly bonded planes simultaneously in grains labeled A and B in (a) and D and E in (b). (c) and (d) Crystallite shape of YAM simulated based on Donnay–Haker theory and viewed in (c) $(0\bar{1}1)$ and (d) (100) directions.

3. 3 Temperature dependence of mechanical properties

To understand the behavior of YAM at high temperatures, the temperature dependence of Young's modulus and strengths were investigated. Figure 4 shows the temperature dependence of Young's modulus and internal friction of YAM. The empirical description of the temperature dependence of Young's modulus is as follows:

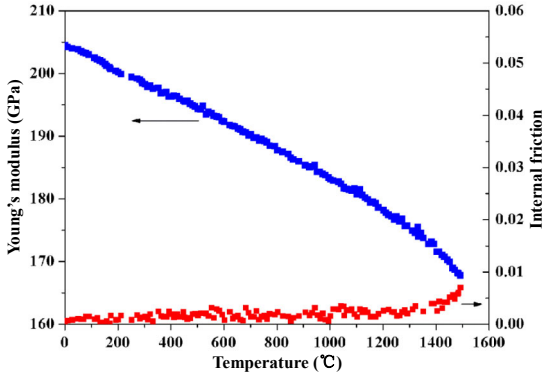

Fig. 4 High-temperature Young's modulus and internal friction of YAM.

$$E = E_0 - bT\exp\left(-\frac{T_0}{T}\right) \tag{6}$$

where E_0 is the Young's modulus at 0 K; T_0 is half of the Debye temperature; and b is an empirical constant. The Debye temperature of YAM is 564 K [2], and b is determined 0.0268 GPa/K. Thus the high-temperature Young's modulus can be described as

$$E = E_0 - 0.0205T\exp\left(-\frac{282}{T}\right) \tag{7}$$

The Young's modulus of YAM linearly decreases with temperature up to a critical temperature $T_c = 1400$ ℃; above T_c, the Young's modulus decreases and the internal friction increases dramatically due to grain boundary sliding. The Young's modulus of YAM at 1400 ℃ (T_c) is 172 GPa, which is about 84% of Young's modulus at room temperature. High T_c and high elevated temperature stiffness indicate that YAM can be used as a promising structural material at high temperatures.

The high-temperature strength of YAM was also investigated. As shown in Fig. 5, the flexure strength keeps almost unchanged up to a critical temperature

$T_c' = 1100$ ℃; above that temperature, the strength of YAM decreases rapidly. At 1200 ℃, the strength of YAM is less than 50% of that at room temperature. The reason for the facts that the critical temperature T_c' is much lower than T_c and the remained strength is much lower than the remained stiffness is not well understood. Figure 6 shows the surface morphology of YAM after high-temperature mechanical property testing at 1200 ℃, where cracks on the surface are obvious. These cracks can act as the origins of fracture during flexural strength testing, which lead to the loss of strength at high temperatures. We can thus conclude that the reduction of strength is due to the cracks formation during rapid furnace heating before testing. The formation of cracks may be due to the anisotropy in elastic stiffness [2] and thermal expansion, which lead to stresses at grain boundaries. The anisotropic elastic properties have been demonstrated in our previous paper [2], and the anisotropic expansion will be discussed in the next section.

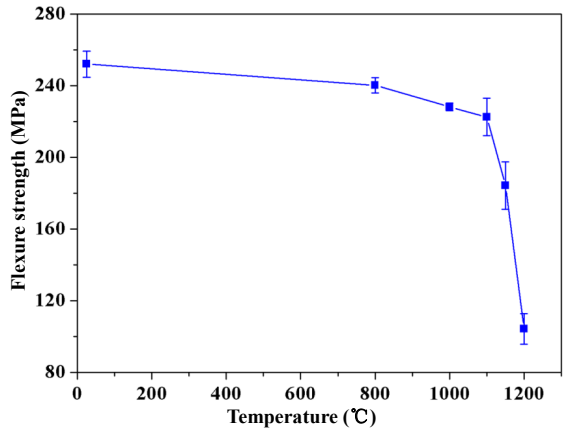

Fig. 5 High-temperature strength of YAM.

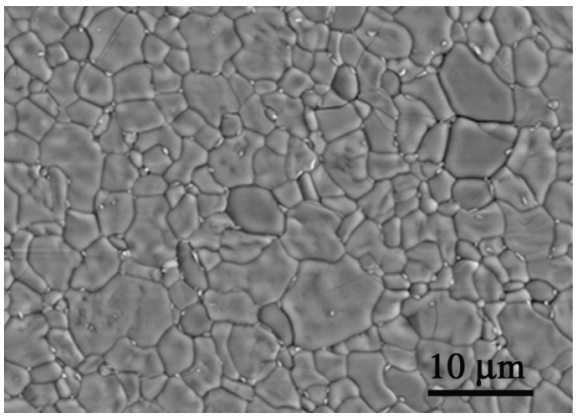

Fig. 6 SEM micrograph of YAM sample surface after high-temperature strength testing at 1200 ℃.

3. 4 Anisotropic thermal expansion behavior

Thermal expansion depends on the strength of the chemical bonds, and the anisotropic chemical bonding in YAM results in anisotropic thermal expansion coefficient as demonstrated in Table 4 of our previous theoretical paper [2]. In this work, the average and anisotropic thermal expansion coefficients of YAM are experimentally investigated. Figure 7 shows the thermal expansion of polycrystalline YAM; wherein the fractional change is almost linear with temperature. The average linear thermal expansion coefficient determined in terms of the slope of thermal expansion versus temperature curve is 7.37×10^{-6} K^{-1}, which is close to the theoretical predicted 7.51×10^{-6} K^{-1} [2].

To investigating the anisotropic thermal expansion behavior, high-temperature XRD patterns collected from 300 K to 1273 K are shown in Fig. 8. In Fig. 8, regular shift of diffraction peaks to the low angles can be clearly seen, indicating the lattice expansion of YAM during heating. Details of the change in lattice parameters with temperature are given in Fig. 9. During heating, *a*, *b*, and *c* axes all slightly increase up to 1073 K. On the other hand, β angle steadily decreases with increasing temperature. The variation of the cell dimensions was fitted to the polynomial equation with the least-squares method:

$$\chi/\chi_{300\mathrm{K}} = 1 + A\Delta T + B(\Delta T)^2 \qquad (8)$$

where χ is the cell dimension at T (K); $\chi_{300\mathrm{K}}$ is the cell dimension at 300 K; and $\Delta T = T - 300$ K. The fitted curves for variation of normalized cell parameters are plotted in Fig. 9, and the constants A and B are given in Table 4. Furthermore, the volumetric and anisotropic thermal expansion coefficients of YAM were obtained. The volumetric

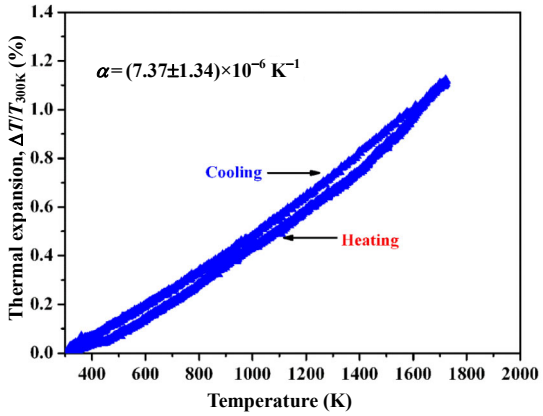

Fig. 7 Thermal expansion coefficient of polycrystalline YAM measured by an optical dilatometer.

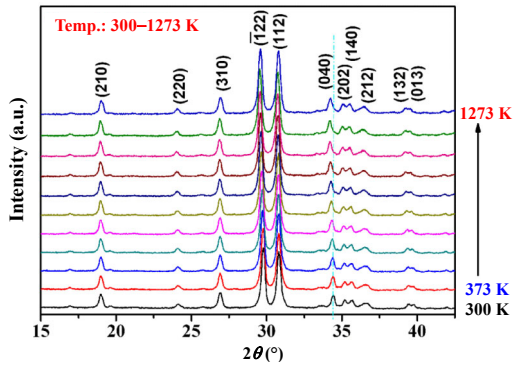

Fig. 8 XRD patterns of YAM powders at 300 K and at high temperatures in the temperature range of 373–1273 K with 100 K increment.

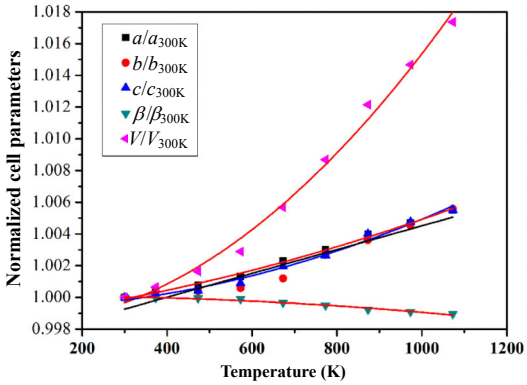

Fig. 9 Variation of normalized cell dimensions (*a*, *b*, *c*, *β*, and *V*) versus temperature.

Table 4 Least-squares fitting results of the normalized cell dimensions for YAM

Phase	Normalized unit cell dimension	$A\times10^{-6}$	$B\times10^{-9}$	R^2
$Y_4Al_2O_9$	a/a_{300K}	3.41	2.89	0.995
	b/b_{300K}	–3.81	8.29	0.983
	c/c_{300K}	0.22	5.43	0.985
	β/β_{300K}	0.26	–1.27	0.971
	V/V_{300K}	–0.56	17.69	0.990

TEC is (23.37±1.61)×10^{-6} K^{-1}, and the anisotropic TEC are $\alpha_a = 7.34\times10^{-6}$ K^{-1}, $\alpha_b = 7.54\times10^{-6}$ K^{-1}, and $\alpha_c = 7.61\times10^{-6}$ K^{-1}. To obtain a clear and complete representation of the anisotropic TEC of $Y_4Al_2O_9$, the variation of TEC as a function of crystal orientation is necessary. The thermal expansion coefficient in an arbitrary direction is given by the following equation:

$$\alpha'_{11} = \alpha_{11}\cos^2\phi\sin^2\theta + \alpha_{22}\sin^2\phi\sin^2\theta + \alpha_{33}\cos^2\theta \quad (9)$$

where θ and ϕ are the spherical coordinate angles. The surface contour of the thermal expansion coefficient of $Y_4Al_2O_9$ is shown in Fig. 10. For $Y_4Al_2O_9$, $\alpha_{22} = \alpha_b$, $\alpha_{33} = \alpha_c$; using Eq. (9), α_{11} is calculated to be 7.31×

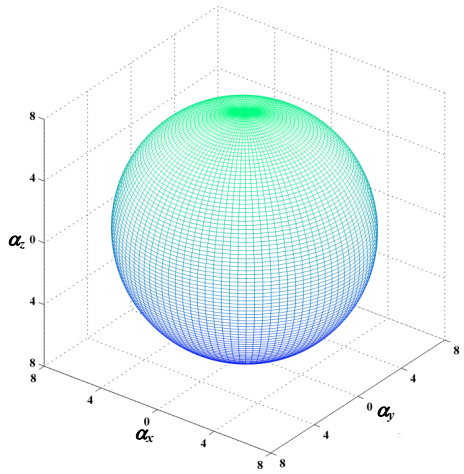

Fig. 10 Surface contour of the thermal expansion coefficient of YAM.

10^{-6} K^{-1}. These data indicate that there is anisotropy in thermal expansion due to the anisotropy in chemical bonding, i.e., strong bonding corresponds to low thermal expansion coefficient.

4 Conclusions

$Y_4Al_2O_9$ (YAM) powders were synthesized by solid-state reaction between Y_2O_3 and Al_2O_3, and the room and high-temperature thermal and mechanical properties of dense YAM were investigated. The measured elastic moduli are close to the theoretical predicted values and the stiffness can be maintained up to 1400 ℃. The flexural strength and fracture toughness are 252.1±7.3 MPa and 3.36±0.20 MPa·$m^{1/2}$, respectively. Damage tolerance of YAM was also experimentally proved. The measured average linear thermal expansion coefficient (TEC) of YAM is 7.37×10^{-6} K^{-1}, which is close to the theoretical predicted value. Using high-temperature XRD analysis, volumetric TEC is determined (23.37±1.61)×10^{-6} K^{-1} and the anisotropic TEC are $\alpha_a = 7.34\times10^{-6}$ K^{-1}, $\alpha_b = 7.54\times10^{-6}$ K^{-1}, and $\alpha_c = 7.61\times10^{-6}$ K^{-1}. In addition, lattice parameters, atomic positions, and a new set of powder XRD pattern of YAM were obtained. The unique combination of low density, low thermal conductivity, and moderate thermal expansion coefficient, Young's modulus, and damage tolerance ability endure YAM a promising material for high-temperature thermal sealing and thermal barrier applications.

Acknowledgements

This work was supported by the National Outstanding Young Scientist Foundation for Y. C. Zhou under Grant No. 59925208, and the National Natural Science Foundation of China under Grant Nos. 50832008 and U1435206.

References

[1] Zhan X, Li Z, Liu B, *et al*. Theoretical prediction of elastic stiffness and minimum lattice thermal conductivity of $Y_3Al_5O_{12}$, $YAlO_3$ and $Y_4Al_2O_9$. *J Am Ceram Soc* 2012, **95**: 1429–1434.

[2] Zhou Y, Xiang H, Lu X, *et al*. Theoretical prediction on mechanical and thermal properties of a promising thermal barrier material: $Y_4Al_2O_9$. *J Adv Ceram* 2015, DOI 10.1007/s40145-015-0140-6.

[3] Li Z, Liu B, Wang JM, *et al*. First-principle study of point defects in stoichiometric and nonstoichiometric $Y_4Al_2O_9$. *J Mater Sci Technol* 2013, **29**: 1161–1165.

[4] Mah T-I, Petry MD. Eutectic composition in the pseudobinary of $Y_4Al_2O_9$ and Y_2O_3. *J Am Ceram Soc* 1992, **75**: 2006–2009.

[5] Zhou X, Xu Z, Fan X, *et al*. $Y_4Al_2O_9$ ceramics as a novel thermal barrier coating material for high temperature applications. *Mater Lett* 2014, **134**: 146–148.

[6] Rietveld HM. Line profiles of neutron powder-diffraction peaks for structure refinement. *Acta Cryst* 1967, **22**: 151–152.

[7] Rietveld HM. A profile refinement method for nuclear and magnetic structures. *J Appl Cryst* 1969, **2**: 65–71.

[8] ASTM International. ASTM E1876-97 Standard test method for dynamic Young's modulus, shear modulus, and Poisson's ratio by impulse excitation of vibration. West Conshohocken, PA, 1998.

[9] Roebben G, Bollen B, Brebels A, *et al*. Impulse excitation apparatus to measure resonant frequencies, elastic moduli, and internal friction at room and high temperature. *Rev Sci Instrum* 1997, **68**: 4511.

[10] He L-F, Bao Y-W, Wang J-Y, *et al*. Mechanical and thermophysical properties of Zr–Al–Si–C ceramics. *J Am Ceram Soc* 2009, **92**: 445–451.

[11] Yamane H, Shimada M, Hunter BA. High temperature neutron diffraction study of $Y_4Al_2O_9$. *J Solid State Chem* 1998, **141**: 466–474.

[12] Chen X-Q, Niu H, Li D, *et al*. Modeling hardness of polycrystalline materials and bulk metallic glasses. *Intermetallics* 2011, **19**: 1275–1281.

[13] Bao YW, Hu CF, Zhou YC. Damage tolerance of nanolayer grained ceramic and quantitative estimation. *Mater Sci Tech* 2006, **22**: 227–230.

[14] Zhou Y-C, Zhao C, Wang F, *et al*. Theoretical prediction and experimental investigation on the thermal and mechanical properties of bulk β-$Yb_2Si_2O_7$. *J Am Ceram Soc* 2013, **96**: 3891–3900.

[15] Sun Z, Zhou YC, Wang JY, *et al*. γ-$Y_2Si_2O_7$, a machinable silicate ceramic: Mechanical properties and machinability. *J Am Ceram Soc* 2007, **90**: 2535–2541.

[16] Zhou Y, Sun Z. Microstructure and mechanism of damage tolerance for Ti_3SiC_2 bulk ceramics. *Mater Res Innov* 1999, **2**: 360–363.

[17] Barsoum MW, El-Raghy T, Ali M. Processing and characterization of Ti_2AlC, Ti_2AlN, and $Ti_2AlC_{0.5}N_{0.5}$. *Metall Mater Trans A* 2000, **31**: 1857–1865.

[18] Li F, Liu B, Wang J, *et al*. Hf_3AlN: A novel layered ternary ceramic with excellent damage tolerance. *J Am Ceram Soc* 2010, **93**: 228–234.

[19] Lin ZJ, Zhuo MJ, Li MS, *et al*. Synthesis and microstructure of layered-ternary Ti_2AlN ceramic. *Scripta Mater* 2007, **56**: 1115–1118.

[20] Wang XH, Zhou YC. Layered machinable and electrically conductive Ti_2AlC and Ti_3AlC_2 ceramics: A review. *J Mater Sci Technol* 2010, **26**: 385–416.

[21] Donnay JDH, Haker D. A new law of crystal morphology extending the law of Bravais. *Am Mineral* 1937, **22**: 446–447.

[22] Wells AF. Crystal habit and internal structure. *Phil Mag* 1946, **37**: 184–199.

[23] Berkovitch-Yellin Z. Toward an *ab initio* derivation of crystal morphology. *J Am Chem Soc* 1985, **107**: 8239–8253.